Molecular Dynamics Simulations of Polyampholyte−Polyelectrolyte Complexes in Solutions

Junhwan Jeon and Andrey V. Dobrynin*

Polymer Program, Institute of Materials Science and Department of Physics, University of Connecticut, Storrs, Connecticut 06269

Received February 11, 2005; Revised Manuscript Received March 31, 2005

ABSTRACT: We have studied how the charge distribution along a polyampholyte backbone influences aggregation of polyampholyte and polyelectrolyte chains in dilute and semidilute solutions. Using molecular dynamics (MD) simulations, we have shown that the complexation between polyampholyte and polyelectrolyte chains is due to polarization-induced attractive interactions between molecules. A polyampholyte chain binds to a polyelectrolyte in such a way to maximize the electrostatic attraction between oppositely charged ionic groups and minimize the electrostatic repulsion between similarly charged ones. The charge sequence along the polyampholyte backbone has a profound effect on the complex structure. In dilute solutions, a diblock polyampholyte could form a three-arm starlike complex in which the longest branches of the star are formed either by two sections of the polyelectrolyte chain or by a negatively charged block of the polyampholyte and by a section of the polyelectrolyte chain. There are no such complexes in solutions of random polyampholytes and polyampholytes with short blocky charge sequences. In dilute solutions of moderate polymer concentration polyampholytes with long blocky charge sequences form mixed micellar aggregates containing both polyampholyte and polyelectrolyte chains. In semidilute solutions diblock polyampholytes form a network of micelles spanning the entire system. On the contrary, the structure of multichain aggregates formed by random polyampholytes and polyelectrolytes resembles that of branched polymers with polyampholyte chains cross-linking polyelectrolytes together. The osmotic coefficients of polyampholyte polyelectrolyte mixtures show no dependence on the charge sequence along the polymer backbone, confirming the leading contribution of small ions to osmotic pressure of ionic systems.

1. Introduction

Complexes between polyelectrolytes and polyampholytes (proteins) play an important role in protein separation,[1−4] biosensor development,[5,6] and enzyme immobilization.[7] They find application as rheology modifiers[8] and drug delivery vessels. Interactions of a protein with DNA are also central to the control of gene expression and nucleic acid metabolism.[9] Electrostatic interactions between oppositely charged groups are the leading factors controlling the complex formation and its structure. The binding between polyelectrolytes and proteins occurs in such a way that oppositely charged amino acids on the protein are close to the polyelectrolyte backbone, causing an electrostatic attraction between the two.[10,11] An example of such complex is the aggregation of single-stranded gelatin (denatured collagen) that exists as a flexible random coil in water above 40 °C, with sodium poly(styrenesulfonate), NaPSS, in aqueous solutions.[12] Another example of complexes of proteins and polyelectrolytes is found in synovial fluid, where the anionic polyelectrolyte sodium hyaluronate binds with a variety of proteins.[13−16]

Recently, Bowman et al.[12] performed a detailed study of complex formation between negatively charged polyelectrolytes sodium poly(styrenesulfonate), NaPSS, and sodium poly(2-acrylamido-2-methylpropanesulfonate), NaPAMS, with single-stranded gelatin in the range of pH above the isoelectric point of gelatin ($pH_{iso} = 4.9$), where the net charge on the protein is negative. Using light scattering, they established that the molecular weight of a single polyelectrolyte chain of NaPSS and NaPAMS increases 20- and 15-fold, respectively, as it complexes with gelatin. The gelatin/polyelectrolyte complex has a negative second virial coefficient, indicating a tendency toward interchain complexation with increasing polymer concentration. Indeed, in semidilute solutions reversible gels (see for review ref 17) are formed.[18] The reversible gel nature plays an important role in the technological applications of such mixtures. For example, addition of a small amount of anionic polyelectrolyte boosts the viscosity of gelatin solutions for coating photographic film and paper.[8]

The electrostatic nature of the association between polyelectrolytes and gelatin is supported by the strong effects of pH and salt concentration on the complex stoichiometry, defined as a ratio of the total molecular weight of adsorbed gelatin molecules per polyelectrolyte chain to the molecular weight of the polyelectrolyte chain. The complex stoichiometry decreases monotonically with increasing pH, since this increases the strength of electrostatic repulsion between the polyelectrolyte and gelatin. At constant pH, the complex stoichiometry shows a nonmonotonic dependence on salt concentration.

Protein−polyelectrolyte affinity maximizes as a function of salt concentration and was confirmed for globular proteins such as bovine serum albumin, insulin, lysozyme, and β-lactoglobulin.[19,20] In this case the protein polarization is associated with alignment of the protein dipole moment in the external electric field of polyelectrolyte chain. Since globular proteins do not change their conformations upon binding, the position of the maximum net attraction is located at the salt concentration for which the corresponding Debye length is approximately half of the protein diameter, so that

* Corresponding author. E-mail: avd@ims.uconn.edu.

10.1021/ma050303j CCC: $30.25
Published on Web 05/12/2005

the salt screens most of the electrostatic repulsion. It is interesting to note that many physiological conditions have a salt concentration of order 0.1 M, where the Debye length is roughly 10 Å, which is comparable to the radius of many globular proteins.

Counterions released from polyelectrolytes[21−24] can also play an important role in controlling the complex formation. A single protein has many positively charged amino acids that can bind to an anionic polyelectrolyte. These positively charged groups partially neutralize the large negative charge that causes counterions to condense on the anionic polyelectrolyte in the absence of protein. This stabilization allows a bound polyampholyte to release multiple counterions from the polyelectrolyte, contributing to a large portion of the binding free energy which is entropic in origin.[24]

There are two different classes of molecular simulations of polyelectrolyte−protein complexes. One is in the realm of biochemistry and biophysics where the dominant theme is DNA−protein binding. Here the main questions are associated with selective recognition of high specificity, essential for protein function, involving high configurational precision. Usually such simulations involve detailed molecular models of DNA, proteins, and solvent where dynamics of the system are studied on the nanosecond time scale (see for review refs 25 and 26). The second class is in the domain of polymer science, where polyelectrolyte−protein (polyampholyte) systems are represented on the level of coarse-grained chain models which significantly extends accessible time scales by sacrificing details of molecular structure.

Carlsson et al.[27] have performed Monte Carlo simulations of complexation of flexible anionic polyelectrolytes with lysozyme. The protein in these simulations was modeled as a charged sphere with a discrete charge distribution inside a sphere corresponding to the charged residues of the native protein conformation. The effect of added salt was included in these simulations by modeling electrostatic interactions with a Yukawa (screened Coulomb) potential. In these simulations, complexation between polyelectrolyte and protein occurred when the protein has a small net charge, even when both the species had the same sign of charge. For ionic strengths $I = 0.05$ and 0.1 M the onset of complexation occurred when the net charge on the protein was roughly −6. No complexation was observed for strongly negatively charged proteins with net charge less than −6. A reentrant complexation transition was found at higher ionic strength ($I = 0.5$ M). For such high ionic strength, even proteins with a net charge of −13 formed a complex with the negatively charged polyelectrolyte. For all ionic strengths considered in these simulations, the protein polarized itself by rotating and bound to the middle of the polyelectrolyte chain.

The effects of chain length, ionic strength, and the strength of short-range interactions on protein−polyelectrolyte complexation were studied in Monte Carlo simulations by Carlsson et al.[28] Here the net protein charge was fixed at +10, corresponding to the net charge of lysozyme at pH = 4.5. The polyelectrolyte chains in these simulations were negatively charged. At low ionic strengths, the strong electrostatic attraction between protein and the polyelectrolyte caused extensive clustering among themselves. Adding more polyelectrolytes to the system resulted in the appearance of a redissolution, with proteins forming soluble complexes with polyelectrolytes. Increasing salt concentration impeded formation of large clusters by screening the attractive interactions. Increasing the affinity between proteins (strong short-range protein−protein interaction) promotes protein−protein aggregation and facilitates large protein−polyelectrolyte cluster formation.

Recently, we studied the effect of charge sequence on complex formation between flexible polyelectrolytes and flexible polyampholytes in dilute salt-free solutions by Monte Carlo simulations.[29] Both polymers were modeled as bead−spring chains of charged Lennard-Jones particles, each consisting of 32 monomers. These simulations have confirmed the polarization origin of complex formation. A polyampholyte chain in a complex is usually located at the *end* of the polyelectrolyte with part of the polyampholyte chain elongated and aligned along the polyelectrolyte backbone. This complex structure between a polarized polyampholyte chain and a polyelectrolyte leads to minimization of the net electrostatic interaction energy. The initially collapsed polyampholytes undergo a globule−coil transition upon forming the complex. Polyampholytes having random charge sequences form stronger complexes with polyelectrolytes than ones with alternating charge sequences, but weaker in comparison to complexes formed with blocky polyampholytes. Flexible polyampholytes with a long blocky sequence form a double helix with the polyelectrolyte at large values of the interaction parameter.

In this paper we address polyampholyte−polyelectrolyte complexes in solutions and study the effects of counterion and polymer concentration and charge sequence along the polyampholyte backbone on the complex structure. To tackle these problems, we carried out molecular dynamics simulations of complex formation in 1:1 mixtures of polyampholyte and polyelectrolyte chains at different polymer concentrations covering both dilute and semidilute regimes.

2. Model and Simulations Details

We studied complexes in 1:1 mixtures of polyelectrolyte (PE) and polyampholyte (PA) chains with explicit counterions confined into a cubic simulation box of size L with periodic boundary conditions. Both PE and PA chains are modeled as bead−spring chains of charged Lennard-Jones particles consisting of $N = 32$ beads with every bead carrying a charge $+e$ or $-e$. All beads of PE chains are negatively charged while PA chains have both positive and negative charged beads with net zero charge on each chain. We studied polyampholytes with random (RPA) and blocky charge sequences along the polymer backbone. Three different classes of block polyampholytes shown in Figure 1 were investigated, including diblock polyampholytes with block length equal to 16 (2B16PA), tetrablock polyampholytes having 8 similarly charged monomers in each block (4B8PA), and finally octablock polyampholyte with block length being equal to 4 repeat units (8B4PA).

All short-range pairwise interactions are modeled by the truncated-shifted Lennard-Jones potential

$$U_{\mathrm{LJ}}(r_{ij}) = \begin{cases} 4\epsilon_{\mathrm{LJ}}\left[\left(\frac{\sigma}{r_{ij}}\right)^{12} - \left(\frac{\sigma}{r_{ij}}\right)^{6} - \left(\frac{\sigma}{r_{\mathrm{cut}}}\right)^{12} - \left(\frac{\sigma}{r_{\mathrm{cut}}}\right)^{6}\right] & r \le r_{\mathrm{cut}} \\ 0 & r > r_{\mathrm{cut}} \end{cases} \quad (1)$$

where r_{ij} is the distance between two interacting ith and jth beads, σ is the bead diameter which is chosen to be

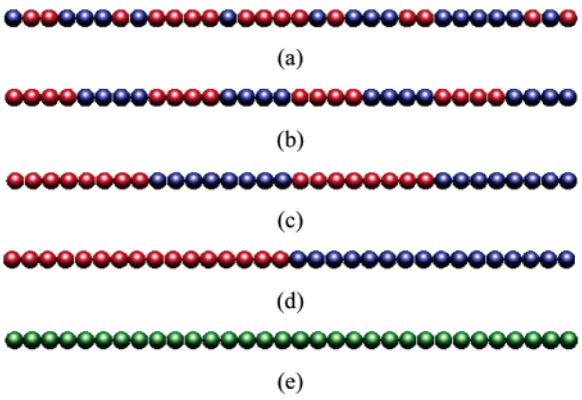

Figure 1. Schematic representation of (a) random polyampholyte chain (RPA), (b) octablock polyampholyte chain (8B4PA), (c) tetrablock polyampholyte chain (4B8PA), (d) diblock polyampholyte chain (2B16PA), and (e) polyelectrolyte chain (PE). The positively charged beads of a polyampholyte chain are shown in red, negatively charged ones are blue, and polyelectrolyte chain is colored in green.

the same regardless of the type of beads, and r_{cut} is a cutoff distance beyond which the interactions are ignored. The cutoff distance r_{cut} is equal 2.5σ for polymer−polymer and $2^{1/6}\sigma$ for polymer−counterion and counterion−counterion interactions. The value of the parameter ϵ_{LJ} which determines the strength of short-range interactions is equal to $\epsilon_{LJ} = 0.35k_BT$, for all pairs, where k_B is the Boltzmann constant and T is the absolute temperature. The value of the parameter $\epsilon_{LJ} = 0.35k_BT$ with $r_{cut} = 2.5\sigma$ between polymeric beads is close to a Θ temperature condition[30] for neutral polymers. This choice of the short-range interaction parameter allows us to study a pure effect of electrostatic interactions on complexation between polyampholyte and polyelectrolyte chains.

The connectivity of beads into polymer chains is maintained by the finite extension nonlinear elastic (FENE) potential

$$U_{FENE}(r) = -0.5k_{spring}R_{max}^{2}\ln\left(1 - \frac{r^2}{R_{max}^{2}}\right) \quad (2)$$

where k_{spring} is the spring constant set to be $k_{spring} = 7k_BT/\sigma^2$ and the maximum bond length is $R_{max} = 2\sigma$. The FENE potential only gives the attractive part of the bond potential while the repulsive part is provided by the truncated-shifted LJ potential given by eq 1.

Solvent presence is taken into account by a dielectric medium with a dielectric constant ϵ. In such a representation, charged beads interact via the Coulomb potential

$$U_{Coul}(r_{ij}) = k_BT\frac{l_Bq_iq_j}{r_{ij}} \quad (3)$$

where q_i is the charge valence of the ith bead bearing a value of ±1. The strength of the electrostatic interactions is described by the Bjerrum length $l_B = e^2/\epsilon k_BT$, defined as the length scale at which the Coulomb interaction between two elementary charges e in a dielectric medium with the dielectric constant ϵ is equal to the thermal energy k_BT. For example, the Bjerrum length is about 7 Å in water at room temperature (298 K). In our simulations, the value of the Bjerrum length l_B is equal to 3σ. The system electroneutrality is maintained by adding monomer-like counterions to compensate for each charge on polyampholyte and polyelectrolyte chains. The electrostatic interactions in our simulations are calculated by the particle−particle particle−mesh (P^3M) method implemented in LAMMPS,[31] which takes into account electrostatic interactions with all periodic images of the system.

Table 1. List of Notations and System's Parameters

simulation box size	L
bead diameter (polymer and counterion)	σ
polymer chain length	$N = 32$
no. of polyampholyte chains	M_{PA}
no. of polyelectrolyte chains	M_{PE}
no. of counterions	M_C
Lennard-Jones interaction parameter	$\epsilon_{LJ} = 0.35k_BT$
Bjerrum length $l_B = e^2/\epsilon k_BT$	$l_B = 3\sigma$
bead charge	$\pm e$
polymer concentration $c_p = N(M_{PA} + M_{PE})/L^3$	c_p
counterion concentration	$c_c = c_p$

Simulations are carried out in a constant number of particles, constant volume, and constant temperature (NVT) ensemble. The constant temperature is achieved by coupling the system to a Langevin thermostat. In this case, the motion of all beads in the system is described by the Langevin equation

$$m\frac{d\vec{v}_i}{dt}(t) = \vec{F}_i(t) - \xi\vec{v}_i(t) + \vec{F}_i^{R}(t) \quad (4)$$

where m is the bead mass, $\vec{v}_i$ is the bead velocity, and $\vec{F}_i$ denotes the net deterministic force acting on the ith bead. The stochastic force $\vec{F}_i^{R}$ has zero average value $\langle\vec{F}_i^{R}(t)\rangle = 0$ and δ-functional correlations $\langle\vec{F}_i^{R}(t)\vec{F}_i^{R}(t')\rangle = 6k_BT\xi\delta(t - t')$. The friction coefficient ξ was set to $\xi = m/\tau_{LJ}$, where τ_{LJ} is the standard LJ time $\tau_{LJ} = \sigma(m/\epsilon_{LJ})^{1/2}$. The velocity-Verlet algorithm with a time step $\Delta t = 0.013\tau_{LJ}$ was used for integration of the equations of motion (4).

Parameters used in our simulations as well as the system summary information are given in Tables 1 and 2. We have performed MD simulations of two different systems. To study the effect of counterion concentration on the complexation between polyampholyte and polyelectrolyte chains in dilute solutions, we have carried out simulations of the polyampholyte and polyelectrolyte chains together with their counterions. The counterion concentration c_c between $10^{-5}\sigma^{-3}$ and $1.5 \times 10^{-2}\sigma^{-3}$ was varied by changing the size of the simulation box and keeping the number of counterions unchanged. The effect of the charge sequence on the formation of the multichain aggregates in dilute and semidilute solutions was studied by performing simulations of 20 polyampholyte $M_{PA} = 20$ and 20 polyelectrolyte $M_{PE} = 20$ chains and their counterions $M_C = 1280$. These simulations have covered the polymer concentration range from $5 \times 10^{-3}\sigma^{-3}$ to $2.5 \times 10^{-1}\sigma^{-3}$. For selected polymer concentrations (see Table 2) we have also performed simulations of the systems with 40 and 120 polyampholytes and polyelectrolyte chains. These simulations have allowed us to investigate a finite system size effect on the complex formation. All simulations were performed as follows. At the beginning of each simulation run, polymers and counterions were distributed randomly in a simulation box, and then the system was equilibrated for 10^6 MD steps. At this point the simulations were continued for another 10^6 MD steps to collect the data for detailed analysis.

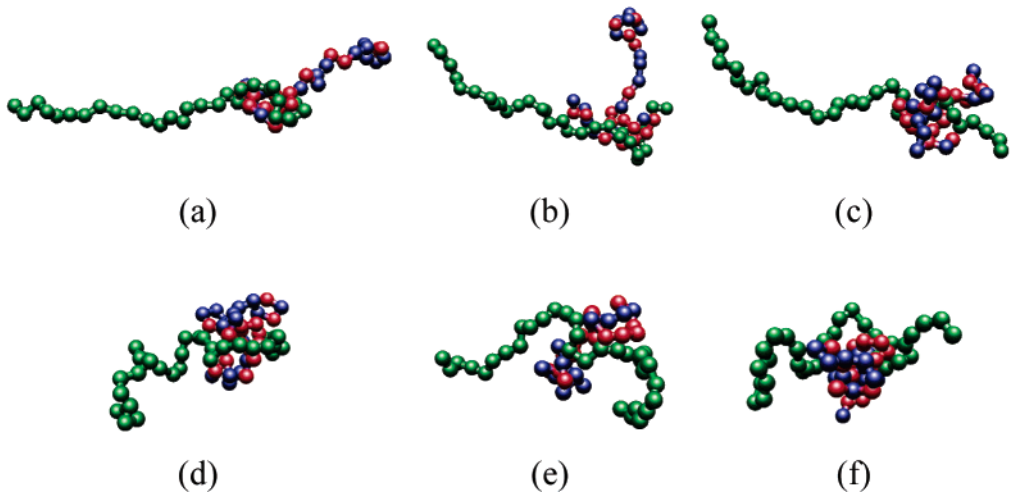

Figure 2. Snapshots of typical conformations of RPA and PE chains in a complex at different counterion concentrations c_c. (a) $c_c = 10^{-5}\sigma^{-3}$; (b) $c_c = 10^{-4}\sigma^{-3}$; (c) $c_c = 5 \times 10^{-4}\sigma^{-3}$; (d) $c_c = 1.5 \times 10^{-3}\sigma^{-3}$; (e) $c_c = 5 \times 10^{-3}\sigma^{-3}$; (f) $c_c = 1.5 \times 10^{-2}\sigma^{-3}$.

Table 2. Summary of Simulated Systems

system	charge sequence of PA	$c_p\sigma^3$	M_{PA}	M_{PE}	M_C
I	RPA, 8B4PA, 4B8PA, 2B16PA	10^{-5}, 10^{-4}, 5×10^{-4}, 1.5×10^{-3}, 5×10^{-3}, 1.5×10^{-2}	1	1	48 (+), 16 (−)
IIa	RPA, 8B4PA, 4B8PA, 2B16PA	5×10^{-3}, 5×10^{-2}, 10^{-1}, 1.5×10^{-1}, 2×10^{-1}, 2.5×10^{-1}	20	20	960 (+), 320 (−)
IIb	RPA, 8B4PA, 4B8PA, 2B16PA	5×10^{-2}, 10^{-1}, 2.5×10^{-1}	40	40	1920 (+), 640 (−)
			120	120	5760 (+), 1920 (−)

3. Simulations Results

3.1. Two-Chain Complex Structure in Dilute Solutions. In very dilute solutions, the most probable complexes are those formed by single polyampholyte and polyelectrolyte chains. Figure 2 shows the evolution of the chain conformations in a random polyampholyte−polyelectrolyte (RPA−PE) complex with increasing counterion concentration. A polyelectrolyte chain, colored in green, is stretched out by electrostatic repulsion between similarly charged monomers. An increasing counterion concentration leads to gradual contraction of the polyelectrolyte chain (see Figure 2). This chain contraction is due to the screening of the intrachain electrostatic interactions by the surrounding counterions. In salt solutions, the electrostatic interactions are exponentially screened at length scales larger than the Debye screening length $r_D = 1/\sqrt{4\pi l_B c_c}$. Increasing the counterion concentration seems to have stronger effect on the positioning of a polyampholyte chain, colored in red (positively charged beads) and blue (negatively charged beads), in a complex than on its size (see Figures 3 and 4). At low counterion concentration, $c_c = 10^{-5}\sigma^{-3}$, a random polyampholyte chain binds close to the end of the polyelectrolyte. This is confirmed by Figure 3 which shows the distribution function for the projection of the center of mass of a polyampholyte chain on the direction of the end-to-end vector of the polyelectrolyte chain, with the origin placed in the polyelectrolyte center of mass. The most probable position (the position of the peak in the distribution function) of the center of mass of a random polyampholyte chain at this counterion concentration is about 7.5σ from the polyelectrolyte center of mass. It is worth pointing out that such complexation has already been observed in our Monte Carlo simulations,[29] which were performed without counterions. The similarity between complex structures seen in both simulations should not be surprising since at low counterion concentrations charges on both chains interact with each other through unscreened electrostatic potentials. Thus, the positioning of a randomly charged polyampholyte chain at the end of the polyelectrolyte minimizes the net electrostatic energy of the complex. However, as counterion concentration increases, the polyampholyte chain moves toward the middle of the polyelectrolyte chain, which is manifested by the shift in the peak position in the distribution function shown in Figure 3a toward the center of mass of the polyelectrolyte chain. Finally, a random polyampholyte settles in the middle of the polyelectrolyte chain at relatively high counterion concentration $c_c = 1.5 \times 10^{-2}\sigma^{-3}$ (see Figure 3a). At such high counterion concentrations, the size of the polyampholyte chain in a complex becomes comparable with the Debye screening length (see Figure 4a).

The reason for conformational change in the complex structure with increasing counterion concentration can be understood by using the charged diblock analogy of a random polyampholyte chain. For a random polyampholyte, the two halves of the chain are carrying the typical charge of the order of $\pm e\sqrt{N/2}$. The random charge sequence chosen in our simulations has half of the chain carrying the excess positive charge $+4e$ and the other half being negatively charged with the excess charge $-4e$ (see Figure 1). In a complex the positively charged half of the polyampholyte chain is in contact with the negatively charged polyelectrolyte backbone, while the negatively charged half is pointing away from the polyelectrolyte backbone (see Figure 2a). Increasing the counterion concentration decreases the Debye screening length, which first weakens the electrostatic repulsion between the polyelectrolyte chain and the negatively charged half of the polyampholyte chain as it is stretched and is located further away from the polyelectrolyte backbone. Screening of the repulsive electrostatic interactions with the remote section of the polyampholyte chain favors its displacement toward the middle of the polyelectrolyte backbone as it maximizes the electrostatic attraction between the positively charged half of the polyampholyte chain and the polyelectrolyte. Qualitatively similar evolution of the complex structure

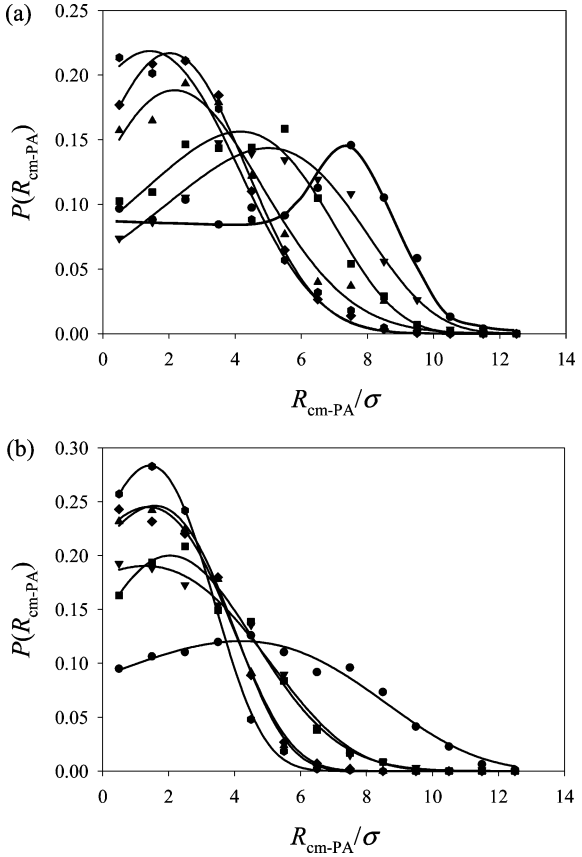

Figure 3. Counterion concentration dependence of the distribution function $P(R_{cm-PA})$ of the position of the center of mass R_{cm-PA} of (a) RPA and (b) 2B16PA polyampholyte chains in a complex. Filled circles, reverse triangles, squares, triangles, diamonds, and hexagons correspond to counterion concentration $c_c = 10^{-5}\sigma^{-3}$, $c_c = 10^{-4}\sigma^{-3}$, $c_c = 5 \times 10^{-4}\sigma^{-3}$, $c_c = 1.5 \times 10^{-3}\sigma^{-3}$, $c_c = 5 \times 10^{-3}\sigma^{-3}$, and $c_c = 1.5 \times 10^{-2}\sigma^{-3}$, respectively.

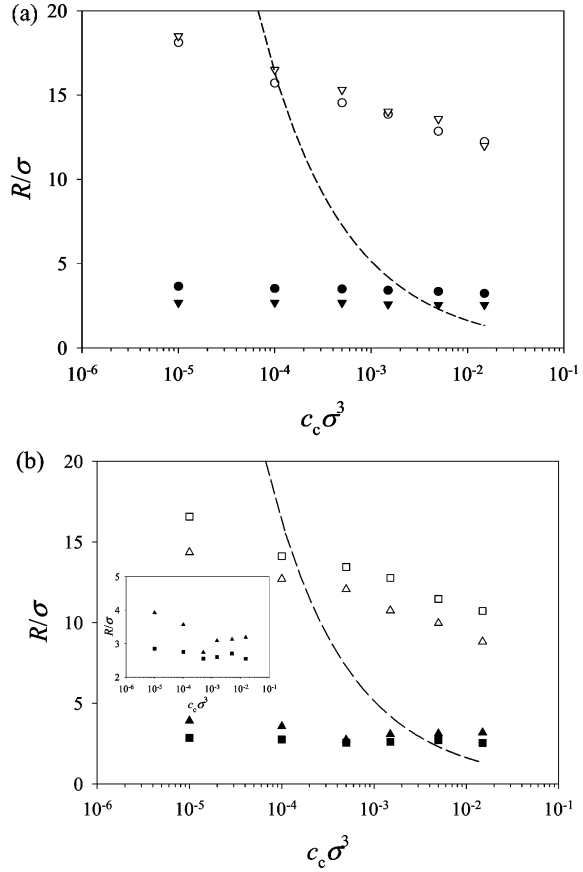

Figure 4. Counterion concentration dependence of the root-mean-square radius of gyration $\langle R_g^2\rangle^{1/2}$ of polyampholyte chain (filled symbols) and of the root-mean-square end-to-end distance $\langle R_g^2\rangle^{1/2}$ of the polyelectrolyte chain (open symbols) (a) in RPA−PE (circles) and 8B4PA−PE (reverse triangles) complexes and (b) in 4B8PA−PE (squares) and 2B16PA−PE (triangles) complexes. The concentration dependence of the Debye screening length r_D is shown by the dashed line. The inset in (b) shows concentration dependence of the root-mean-square radius of gyration of block polyampholytes 4B8PA and 2B16PA in a complex.

is expected for a rigid dipole when the Debye screening length becomes smaller than the distance between centers of the dipole's positive and negative charges. This is in agreement with the results of Monte Carlo simulations of complexation between flexible polyelectrolyte and lysozyme performed by Carlson et al.[27] They have found that for high ionic strengths above 0.05 M a protein polarizes by rotating and always binds at the middle of the polyelectrolyte chain.

Complexes formed by block polyampholytes with relatively short blocky charge sequences (8B4PA) show qualitatively similar evolution pattern with increasing counterion concentration as was observed for the random polyampholyte. For all these systems, a polyampholyte chain is initially located at the end of a polyelectrolyte backbone and then moves toward the middle of the polyelectrolyte as the counterion concentration increases. During this journey, the dimensions of both chains forming a complex change gradually with increasing counterion concentration.

A qualitatively different behavior is seen in Figure 4b for concentration dependence of the size of the tetrablock (4B8PA) and diblock (2B16PA) polyampholytes. Both polyampholytes show nonmonotonic dependences of the polyampholyte chain size on the counterion concentration. Consequently, for these polyampholytes, two different complex structures coexist at the same time. This is clearly seen in the distribution function of the square root of the mean-square radius of gyration of a polyampholyte chain shown in Figure 5. The distribution function $P(R_g)$ of the diblock polyampholyte has two well-separated maxima which correspond to a three-arm star complex structure between the polyampholyte and polyelectrolyte chains (see Figure 5a). (The distribution function for a tetrablock polyampholyte (see Figure 5b) does not show a clear separation between these two complex conformations, but it is much broader than that for the block polyampholyte (8B4PA) shown in Figure 5c.) In the three-arm complex the two longest arms of a star can be formed either by two sections of polyelectrolyte chain or by sections of polyelectrolyte and polyampholyte chains. The three-arm star complex where the two longest arms contain polyelectrolyte monomers has a lower electrostatic energy than that of a complex that has two longest arms composed of polyelectrolyte and polyampholyte monomers. This is manifested by the larger magnitude of the first peak in the distribution function $P(R_g)$. These two complexes continue to coexist at a counterion concentration $c_c = 10^{-4}\sigma^{-3}$, while for higher counterion concentrations there is only one peak in the distribution function $P(R_g)$. At these counterion concentrations, the complex favors an almost symmetric starlike conformation. This complex structure becomes more favorable when the Debye radius becomes comparable with half of the

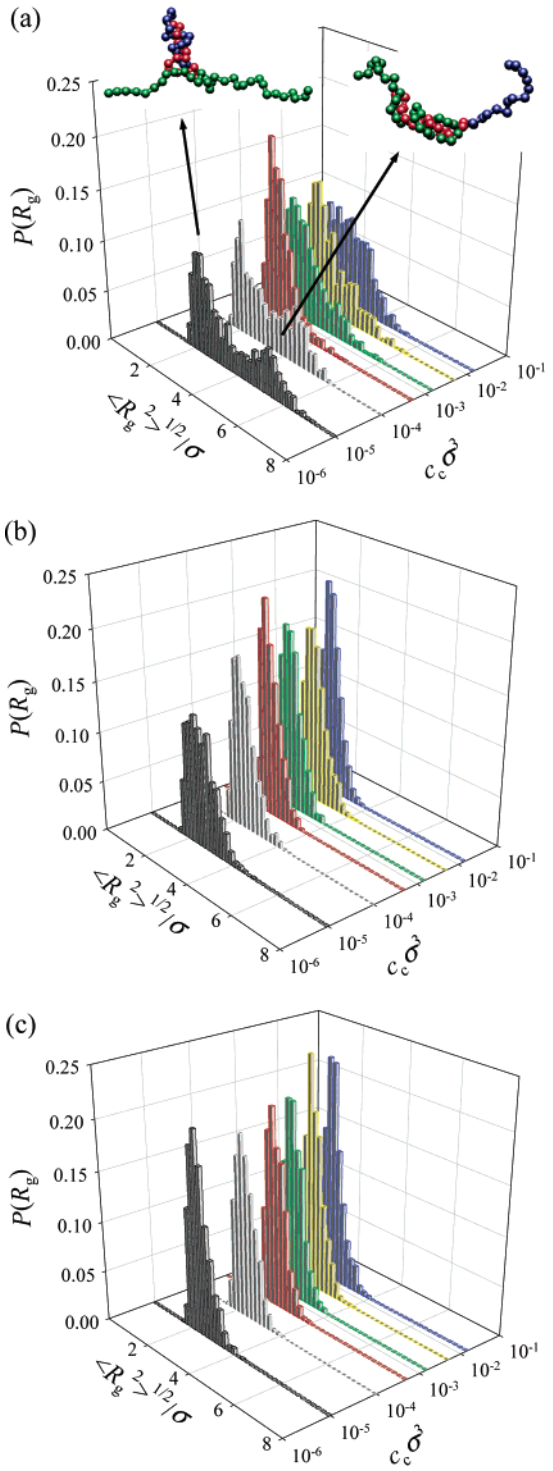

Figure 5. Distribution function $P(R_g)$ of the square root of the mean-square radius of gyration of polyampholyte chains in complexes: (a) diblock polyampholyte (2B16PA); (b) tetrablock polyampholyte (4B8PA); (c) octablock polyampholyte (8B4PA).

polyelectrolyte chain size. Thus, nonmonotonic dependence of the polyampholyte chain size on the counterion concentration is a result of the ensemble averaging over the bimodal distribution function.

3.2. Flory Theory of Two-Chain Polyampholyte−Polyelectrolyte Complex. The evolution of conformational change in the complex structure can be followed by considering a Flory-like model of the complex. In this model, partitioning of chain's sections between arms of a star is determined by the fine interplay between the

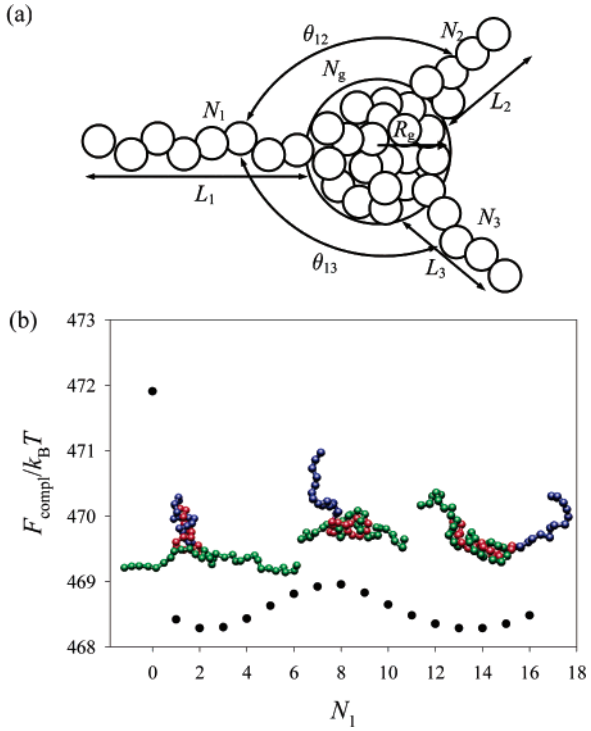

Figure 6. (a) Schematic sketch of a three-arm starlike complex and (b) dependence of the optimized free energy of the three-arm complex on the number of monomers in an arm formed by negatively charged polyampholyte block calculated for $l_B = 3\sigma$ and $c_c = 10^{-5}\sigma^{-3}$.

elastic energy of the arms of a star, star electrostatic energy, and surface as well as bulk energies of the central collapsed bead. The collapse of the central bead is caused by fluctuation-induced attractive interactions between charged monomers.

Consider a three-arm starlike complex (see Figure 6a) with the number of monomers in each arm N_1, N_2, and N_3. We assign N_1 to be the number of monomers in the negatively charged polyampholyte block and consider the variation of the complex free energy as a function of the number of monomers in polyampholyte arm. Two other arms of a star are formed by two ends of the polyelectrolyte chain. The arms of the star are aligned with respect to each other with angles θ_{12} and θ_{13}. The length of an arm with N_i monomers is equal to L_i. The central bead of the star is a collapsed globule consisting of N_g monomers

$$N_g = 2N - N_1 - N_2 - N_3 \tag{5}$$

with size

$$R_g \approx \sigma N_g^{1/3} \tag{6}$$

The net charge of the globule is equal to

$$\Delta N_g = N_1 + N_2 + N_3 - N \tag{7}$$

The free energy of the three-arm star complex is equal to

$$F_{compl} = F_{elast} + U_{electr} + U_{glob} + U_{surf} \tag{8}$$

where the first term is the elastic energy of the arms

$$\frac{F_{\text{elast}}}{k_{\text{B}}T} = \sum_i N_i \left(\beta_i \coth(\beta_i) - \ln\left(\frac{\sinh(\beta_i)}{\beta_i}\right) - 1 \right) \quad (9)$$

and parameter β_i is related to the arm length L_i by the following equation

$$L_i = N_i \sigma (\coth(\beta_i) - 1/\beta_i) \quad (10)$$

The second term in the eq 8 is the electrostatic energy of a complex

$$\frac{U_{\text{electr}}}{k_{\text{B}}T} = \frac{l_{\text{B}} \Delta N_{\text{g}}^{\,2}}{2R_{\text{g}}(1 + R_{\text{g}}/r_{\text{D}})} + \frac{l_{\text{B}}}{2} \sum_i \left(\frac{N_i}{L_i}\right)^2 \int_0^{L_i} \int_0^{L_i} \frac{ds_1\, ds_2}{|s_1 - s_2|} \exp\left(-\frac{|s_1 - s_2|}{r_{\text{D}}}\right) + l_{\text{B}} \Delta N_{\text{g}} \sum_i \frac{N_i}{L_i} \int_{R_{\text{g}}}^{L_i + R_{\text{g}}} \frac{ds_1}{s_1} \exp\left(-\frac{s_1}{r_{\text{D}}}\right) + l_{\text{B}} \Delta N_{\text{g}} \sum_{i<j} \frac{N_i N_j}{L_i L_j} \int_{R_{\text{g}}}^{L_i + R_{\text{g}}} \int_{R_{\text{g}}}^{L_j + R_{\text{g}}} \frac{ds_1\, ds_2}{\sqrt{s_1^{\,2} + s_2^{\,2} - 2 s_1 s_2 \cos(\theta_{ij})}} \times \exp\left(-\frac{\sqrt{s_1^{\,2} + s_2^{\,2} - 2 s_1 s_2 \cos(\theta_{ij})}}{r_{\text{D}}}\right) \quad (11)$$

where s_i is the coordinate along the ith arm elongation axis and r_{D} is the Debye radius. The third and fourth terms in the eq 8 describe the bulk and surface energies of the central globule

$$U_{\text{glob}} + U_{\text{surf}} \approx -k_{\text{B}}T \epsilon_{\text{g}} N_{\text{g}} + 4\pi R_{\text{g}}^{\,2} \gamma \quad (12)$$

where ϵ_{g} is the cohesive energy of the globule formed by oppositely charged monomers and γ is the globular surface energy. The surface energy of the globule can be estimated as $\gamma \approx 2k_{\text{B}}T\epsilon_{\text{g}}/(\pi\sigma^2)$. The magnitude of the cohesive energy is proportional to $\epsilon_{\text{g}} \approx l_{\text{B}} \rho_{\text{g}}^{-1/3}$, where ρ_{g} is the monomer density inside the globule. In our calculations, we will assume that the globule is dense such that $\rho_{\text{g}}\sigma^3 \approx 1$. To find the optimal distribution of monomers between the globule and the arms at a fixed number of monomers in the polyampholyte arm N_1, the total free energy of the globule eq 8 is minimized with respect to the parameters β_i, θ_{12}, θ_{13}, N_2, and N_3.

Optimization of the free energy of the complex leads to the coexistence of two distinct minima in the complex free energy (see Figure 6b). One minimum corresponds to an asymmetric star complex in which the two longest arms are formed by a section of polyelectrolyte and by a part of the negatively charged polyampholyte block. Another one is a star with two longest arms formed by sections of a polyelectrolyte chain and the small arm corresponding to a short section of the polyampholyte block. In both complexes the central collapsed bead has very small excess charge. Placement of the almost neutral bead in the middle of the complex minimizes the net electrostatic energy of the aggregate. The coexistence of these two complex structures is a result of a perfect match between the number of monomers in a polyampholyte block and the number of monomers in one-half of the polyelectrolyte chain. The two longest arms of a starlike complex can be formed either by two polyelectrolyte tails or by sections of polyelectrolyte and a negatively charged polyampholyte block. The appearance of the small third arm is a result of compensation of the charge of the central bead by a section of polyelectrolyte chain. To form two tails at opposite sides of the central bead, the polyelectrolyte chain should have a finite number of monomers inside a globule, thus contributing some charge to its charge neutralization. Thus, to keep the collapsed bead neutral, the same number of monomers belonging to the negatively charged block should be expelled from the bead. Even for tetrablock polyampholytes, there exists a possibility for two different complex structures. However, the two longest arms of a starlike complex in this case are strongly asymmetric because of the difference in the number of monomers in one-half of polyelectrolyte chain and in the blocky charge sequence of polyampholyte. For even shorter blocks only one complex structure corresponds to a free energy minimum of the aggregate. In the case of random polyampholytes, the symmetry between chains is broken by the effective charge density of halves of the chains. For a random polyampholyte, the typical excess charge of a half of a chain is on the order of $\sqrt{N}$. This leads to the effective fraction of negatively charged monomers to be $1/\sqrt{N}$.

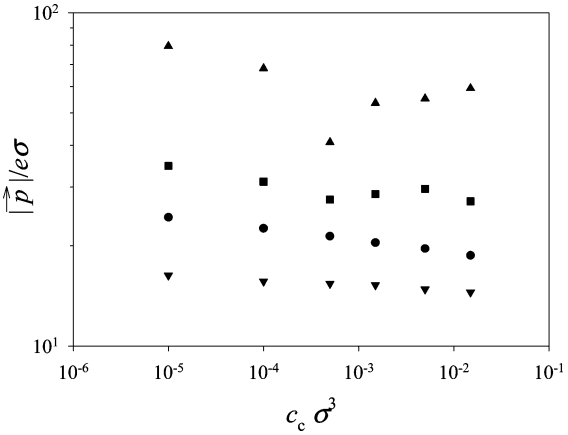

Figure 7. Counterion concentration dependence of the absolute value of the dipole moment of polyampholyte chain in a complex. Notations are the same as in Figure 4.

3.3. Chain's Polarization in Very Dilute Solutions. The polarizibility of the polyampholyte chain in a complex is described by the electric dipole moment, defined as $\vec{p} = \sum_{i=1}^{N} e q_i \vec{r}_i$. The absolute value of the electric dipole moment $|\vec{p}|$ shows how far the center of mass of the positively charged section of a polyampholyte is located from its negatively charged counterpart. It characterizes both the complex structure and the strength of the electrostatic interactions between polyelectrolyte and polyampholyte chains. The more deformed (polarized) the polyampholyte chain is, the larger absolute value of the electric dipole moment $|\vec{p}|$ it has. Figure 7 shows the variation of the absolute value of the chain's dipole moment $|\vec{p}|$ with counterion concentration. A continuous decrease in the chain polarizability is observed for random polyampholytes as well as for polyampholytes with short blocky charged sequences (8B4PA). Polyampholytes with intermediate (4B8PA) and long blocky charge sequences (2B16PA) undergo a structural transition that is manifested by the change in the chain's dipole moment counterion

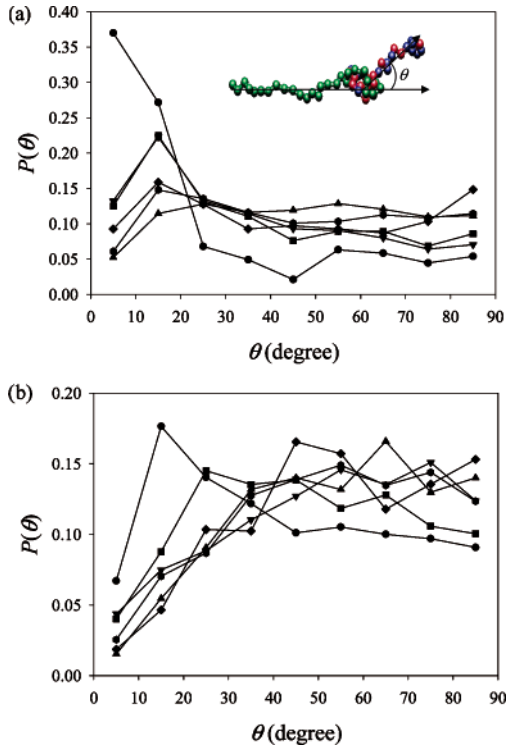

Figure 8. Distribution function $P(\theta)$ of the angle θ between PE end-to-end axis and the direction of the dipole moment of (a) random polyampholyte (RPA) and (b) diblock polyampholyte (2B16PA). Notations are the same as in Figure 3.

concentration dependence at $c_c = 5 \times 10^{-4}\sigma^{-3}$. This structural change in polyampholyte conformation has already been seen in Figure 4b, which shows the concentration dependence of the polyampholyte chain size. At this counterion concentration, the Debye screening length becomes comparable with the polyelectrolyte chain size. This leads to screening of the electrostatic repulsion between polyelectrolyte and similarly charged sections of the polyampholyte chain, causing reduction in the absolute value of the dipole moment $|\vec{p}|$. Further increase in counterion concentration leads to the screening of electrostatic attraction between polyelectrolyte and oppositely charged sections of polyampholyte. A polyelectrolyte chain can effectively increase electrostatic attraction by entering inside a collapsed polyampholyte chain. The charge balance inside a complex leads to the expulsion of similarly charged polyampholyte block out of the collapsed polyampholyte chain section. Such redistribution of the negative charge in the system maximizes the electrostatic attraction and minimizes the electrostatic repulsion. This complex structure results in an increase of the absolute value of the dipole $|\vec{p}|$. This explanation is consistent with the sea gull shape of the function describing the evolution of the absolute value of the dipole moment $|\vec{p}|$ of block polyampholytes 4B8PA and 2B16PA with counterion concentration.

The mutual orientation of the dipole moment $\vec{p}$ of a polyampholyte and the direction of the end-to-end vector of polyelectrolyte chain is described by the angle θ (see Figure 8). At very low counterion concentration $c_c = 10^{-5}\sigma^{-3}$, a random polyampholyte chain is aligned along the polyelectrolyte backbone which is confirmed by a high probability of small angles, $0° \le \theta \le 15°$, in the angle distribution function shown in Figure 8a. With increasing counterion concentration, the angle distribution function broadens by increasing the probability of wider angles. Finally, at counterion concentrations above $c_c = 5 \times 10^{-4}\sigma^{-3}$ the orientational preference in the direction of the dipole moment is lost, indicating that the electrostatic repulsion between negatively charged sections of RPA and PE is completely screened. On the contrary, since 2B16PA moves toward the middle of the PE at lower counterion concentration, $c_c \approx 10^{-4}\sigma^{-3}$, to form a three-arm starlike structure, large angle values are always found for this block polyampholytes with relatively high probability in comparison with that for random polyampholytes at higher counterion concentrations $c_c \ge 10^{-4}\sigma^{-3}$.

3.4. Formation of Multichain Aggregates in Dilute and Semidilute Solutions. With increasing polymer concentration, multichain aggregates begin to appear in a solution. At low polymer concentration $c_p = 5 \times 10^{-3}\sigma^{-3}$, one or a few random polyampholytes can bind to a single polyelectrolyte, thus leaving behind unassociated polyelectrolyte chains. As the system becomes denser, multichain aggregates consisting of polyelectrolyte and polyampholyte chains are found with high probability. The structure of multichain polyampholyte−polyelectrolyte complexes in this case resembles that of branched polymers with polyampholyte backbones binding together polyelectrolyte chains. Finally, at very high polymer concentration $c_p = 2.5 \times 10^{-1}\sigma^{-3}$ almost all chains form an interconnected network which spans the entire system.

A qualitatively different picture of the evolution of the aggregate structure is seen for block polyampholytes with long blocky charge sequences like 2B16PA and 4B8PA. At low polymer concentration $c_p = 5 \times 10^{-3}\sigma^{-3}$ these form small aggregates containing a couple polymer chains. As polymer concentration increases to $c_p = 1.5 \times 10^{-2}\sigma^{-3}$, micellar aggregates, which consists of densely packed inner core and sparsely packed outer corona, appear in a system. A micelle contains both polyampholyte and polyelectrolyte chains. The equilibrium aggregation number of these micelles is controlled by a fine interplay between fluctuation-induced attractive interactions between oppositely charged sections of the chains forming a micellar core and electrostatic repulsion between ionized groups in the corona of the micelle. The micellar aggregates persist until the system crosses over to semidilute regime at $c_p = 0.1\sigma^{-3}$ where all chains form interconnected network of micelles.

Figure 9 shows the evolution of the distribution function of the number of chains N_{agg}, forming an aggregate with polymer concentration. (A chain is considered to belong to a cluster if there is at least one monomer of this chain within a distance of 1.1σ from a monomer belonging to an aggregate.) At a polymer concentration $c_p = 5 \times 10^{-3}\sigma^{-3}$, the most probable aggregates are those that consist of less than six chains regardless of the charge sequence along the polyampholyte backbone. With increasing polymer concentration, the fraction of small aggregates ($N_{agg} \le 6$) decreases while that of large aggregates ($N_{agg} \ge 20$) increases. This is manifested by the appearance of a new peak in the distribution function located at the range of large aggregation numbers N_{agg}. As one would expect, more polarizable polyampholytes[29] such as 4B8PA and 2B16PA form larger aggregates at relatively low polymer concentration than random polyampholytes and those with short charged blocks like 8B4PA. For diblock polyampholytes 2B16PA the second peak in the distribution

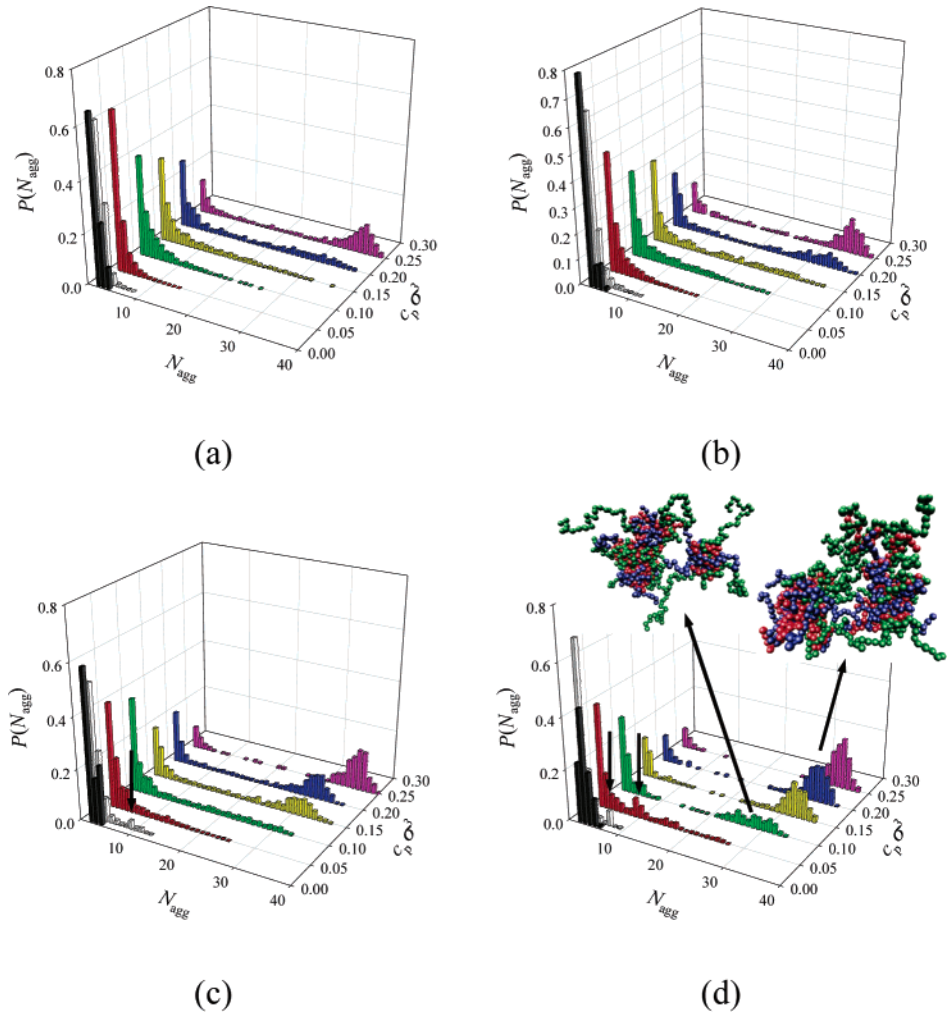

Figure 9. Distribution function $P(N_{agg})$ of the number of chains in an aggregate N_{agg} at different polymer concentration c_p: (a) RPA−PE; (b) 8B4PA−PE; (c) 4B8PA−PE; (d) 2B16PA−PE systems.

function located at $N_{agg} \approx 9$ appears at polymer concentrations $c_p = 1.5 \times 10^{-2}\sigma^{-3}$ and $c_p = 5 \times 10^{-2}\sigma^{-3}$. The magnitude of this peak is lower than that of the two-chain complex. The appearance of the second peak in the distribution function of the number of chains in an aggregate is an indication that a system approaches the critical aggregation concentration, above which most of the polymeric mass is stored inside micelles. Unfortunately, for our system the critical aggregation concentration is close to the cluster overlap concentration and cannot be precisely identified. Figure 10 shows the typical aggregate structures formed by nine polyampholyte and polyelectrolyte chains. As one can see, block polyampholytes 4B8PA and 2B16PA form micellar aggregates while random and 8B4PA polyampholytes form branch polymer-like aggregates.

At very high polymer concentration $c_p = 2.5 \times 10^{-1}\sigma^{-3}$, the most probable aggregates are those with the number of chains between $N_{agg} = 30$ and $N_{agg} = 40$. These aggregates are formed by all the 20 polyampholytes while the number of polyelectrolyte chains can vary between 10 and 20 chains. At this polymer concentration the system forms a semidilute polymer solution with a cluster of chains (network of micelles) spanning the entire system.

To ensure that the aggregates formed in the solution indeed correspond to equilibrium structures, we have performed two sets of simulations starting from different initial configurations. In simulation number one, both polyampholyte and polyelectrolyte chains were uniformly distributed over the system volume. The second simulation was started by placing only polyampholytes and their counterions into the simulation box, and then the system was equilibrated for 10^6 MD steps. After the equilibration procedure was completed, all the polyampholyte chains form one huge aggregate. At this stage polyelectrolyte chains and their counterions were uniformly distributed over the remaining volume of the simulation box, and the simulation was continued for 2×10^6 MD steps. Both simulation runs produced identical ensemble averages, proving the fact that the aggregates observed in our simulations are equilibrium structures.

Figure 11 shows the concentration dependence of the weight-average number of chains $\langle N_W^{agg} \rangle$ in aggregate on polymer concentration c_p. For block polyampholytes 4B8PA and 2B16PA these curves have an s-like shape, indicating that the larger aggregates are formed from the smaller aggregates with well-defined aggregation number. The saturation of the aggregation number at about 30 chains shows that all 20 polyampholyte chains are participating in the cluster formation. This preserves 2:1 ratio of polyampholyte to polyelectrolyte chains in large aggregates, and it is the same ratio as inside single micelles. Qualitatively different behavior is seen for random and 8B4PA polyampholytes. In this

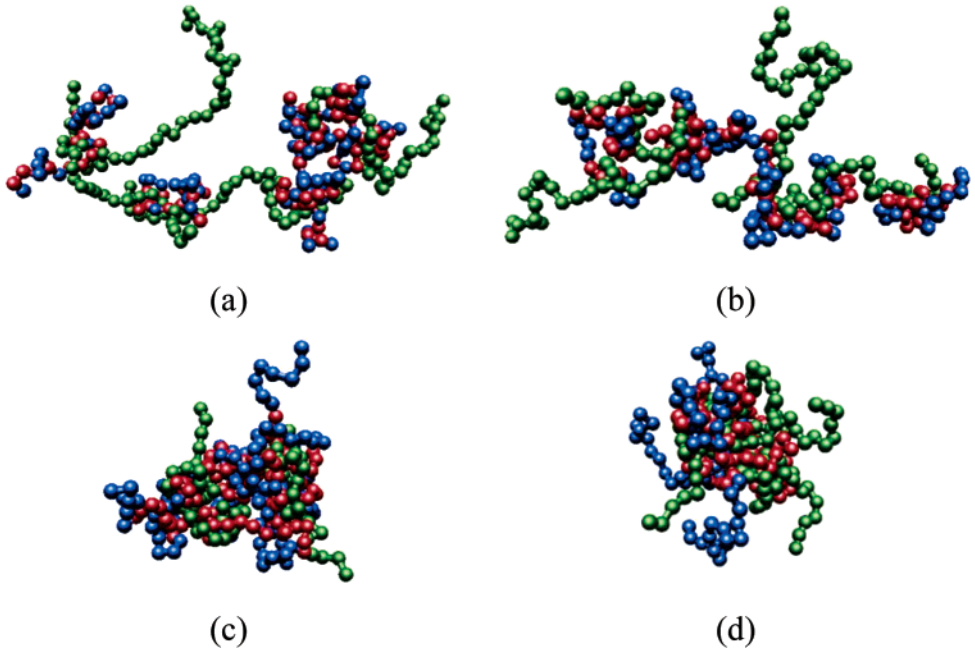

Figure 10. Snapshots of aggregates with aggregation number $N_{agg} = 9$ formed by (a) RPA−PE, (b) 8B4PA−PE, (c) 4B8PA−PE, and (d) 2B16PA−PE chains at polymer concentration $c_p = 0.05\sigma^{-3}$.

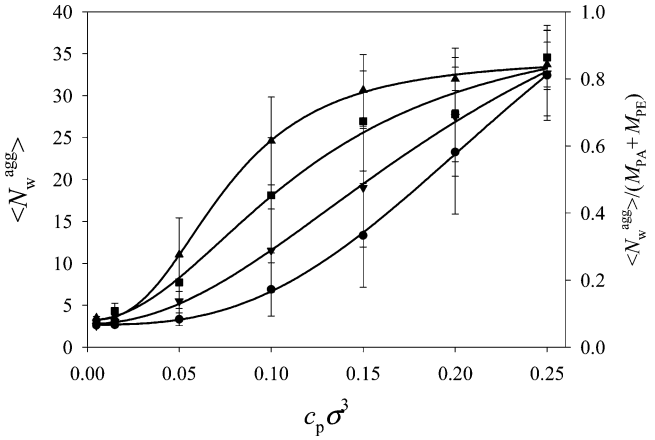

Figure 11. Dependence of the weight-averaged $\langle N_W^{agg} \rangle$ number of chains in aggregate formed by RPA−PE, 8B4PA−PE, 4B8PA−PE, and 2B16PA−PE chains on the polymer concentration. Notations are the same as in Figure 4.

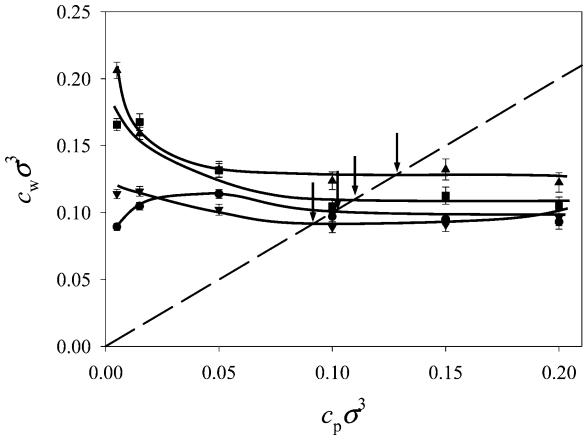

Figure 12. Concentration dependence of the weight-average polymer concentration inside aggregates formed by RPA−PE, 8B4PA−PE, 4B8PA−PE, and 2B16PA−PE chains. Arrows show location of the overlap concentration and a dashed straight line corresponds to $c_W = c_p$. Notations are the same as in Figure 4.

case the aggregation number continue to grow with polymer concentration, indicating that more and more chains are accommodated inside a cluster, and the ratio of polyampholyte and polyelectrolyte chains in aggregates changes with polymer concentration.

The crossover to semidilute solution regime occurs at polymer concentration at which the distance between cluster's center of mass becomes of the order of the cluster size. In polydisperse polymeric system the overlap concentration can be estimated from the weight-average monomer concentration inside clusters

$$\langle c_W \rangle \approx \left\langle \frac{1}{N(M_{PE} + M_{PA})} \sum_{n_{agg}} \frac{(NN_{agg})^2}{R_{max}(N_{agg})^3} \right\rangle \qquad (13)$$

where the brackets $\langle ... \rangle$ denote the ensemble average and summation over n_{agg} is taken over all aggregates in the system and $R_{max}(N_{agg})$ is the distances form the aggregate's center of mass to its furthest monomer. The crossover to the semidilute solution regime occurs at a polymer concentration c_p where the average polymer concentration becomes of the order of polymer concentration inside aggregates $c_W(c_p^*)$. Thus, for all four polyampholyte systems the crossover to semidilute solution regime takes place at relatively high polymer concentrations $c_p^* \approx 0.1-0.15\sigma^{-3}$, as shown in Figure 12.

The polymer density profile inside micellar aggregates in dilute solutions is shown in Figure 13. The monomer density is higher inside the core and gradually decreases toward the corona part of the micelle. The core of the micelle is comprised of an equal number of positively and negatively charged monomers which is manifested by almost zero value of the charge density $Q(r)$ inside the region $r < 3\sigma$, as shown in Figure 14. The corona of the micelle is located at the distances r larger than 3σ from the center of mass of the micelle. It has sections of both polyelectrolyte and polyampholyte chains. The corona of the micelle is negatively charged. All micelles

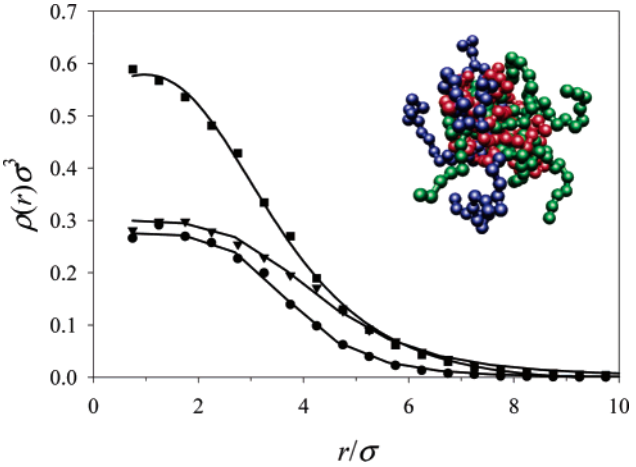

Figure 13. Radial polymer density distribution inside micelles formed by diblock polyampholyte and polyelectrolyte chains at polymer concentration $c_p = 0.05\sigma^{-3}$. Squares show variation of total polymer density, inverse triangles the density of polyampholyte chains, and circles the density of polyelectrolyte chains.

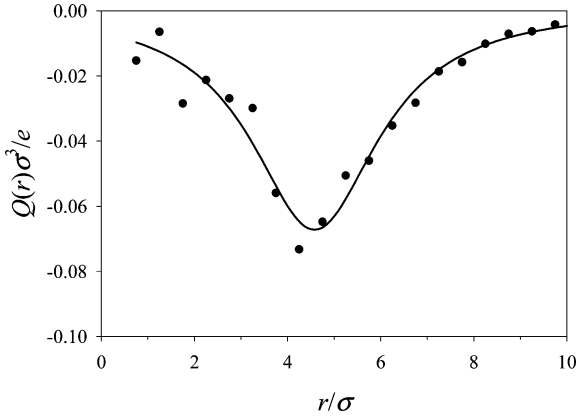

Figure 14. Radial charge density distribution $Q(r)$ inside micelles formed by diblock polyampholyte and polyelectrolyte chains at polymer concentration $c_p = 0.05\sigma^{-3}$.

observed in our simulations are asymmetric, consisting of six polyampholyte and three polyelectrolyte chains.

The composition of aggregates in solutions was monitored by calculating the average number of polyampholyte chains in each aggregate during simulation runs at different polymer concentrations (see Figure 15). Solid lines drawn in Figure 15 correspond to the fraction of polyampholyte chains in aggregates and are equal to $f_{PA} = 0.67$, 0.5, and 0.33 from top to bottom. As one can see, most aggregates formed by polyampholytes and polyelectrolytes reside between the 1:1 ($f_{PA} = 0.5$) and 2:1 ($f_{PA} = 0.67$) ratio. The composition of an aggregate depends on the total number of chains in the aggregate and charge sequence along polyampholyte backbone. Aggregates with fraction of polyampholyte chains ($0.5 < f_{PA} < 0.67$) are most probable to find among aggregates with the total number of chains more than 10 ($N_{agg} > 10$). Polyampholyte chains with long blocky charge sequences like diblock polyampholytes chains are capable of forming strongly asymmetric aggregates with both higher ($f_{PA} > 0.67$) and lower ($f_{PA} < 0.33$) polyampholyte content, as shown in Figure 15b. This is due to the symmetry between block length of polyampholyte chain and half-length of the polyelectrolyte that makes two chain sections mutually interchangeable. To check that the complex composition observed in our simulations is not influenced by the finite system size, we performed simulations of the system consisting of 80 and 240 chains. In all these simulations we have found a similar distribution of the aggregate composition with the total number of chains in an aggregate.

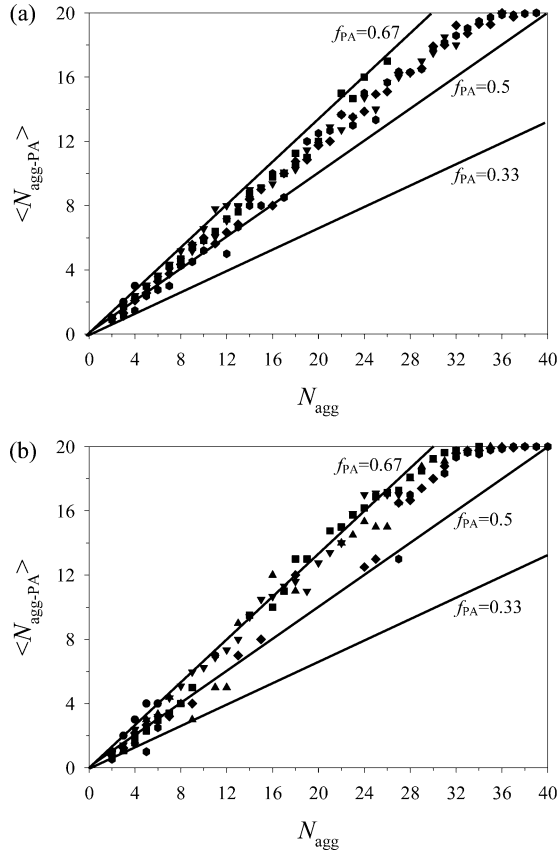

Figure 15. Dependence of the average number of polyampholyte chains $\langle N_{agg-PA} \rangle$ on the total number of chains in an aggregate formed by (a) RPA−PE and (b) 2B16PA−PE chains at different polymer concentrations $c_p = 5 \times 10^{-3}\sigma^{-3}$ (circles), $c_p = 5 \times 10^{-2}\sigma^{-3}$ (reverse triangles), $c_p = 10^{-1}\sigma^{-3}$ (squares), $c_p = 1.5 \times 10^{-1}\sigma^{-3}$ (triangles), $c_p = 2 \times 10^{-1}\sigma^{-3}$ (diamonds), and $c_p = 2.5 \times 10^{-1}\sigma^{-3}$ (hexagons). Solid lines correspond to the fraction of polyampholyte chains in aggregate $f_{PA} = 0.67$, 0.5, and 0.33 from top to bottom.

The preferential binding between a positively charged block of a polyampholyte chain and a polyelectrolyte is confirmed by the charge−charge correlation function $g_{PA+,PE-}(r)$ plotted in Figure 16. The position of the first peak at $r = \sigma$ corresponds to a point of the physical contact of oppositely charged beads and can be interpreted as a formation of ionic pairs. This peak persists for all polymer concentrations, thus confirming the leading role of the ionic pairs in the aggregate formation. The secondary peak is located at about $r = 1.8\sigma$ and corresponds to a correlation of the selected charged bead with two nearest monomers along the polyelectrolyte backbone from one participating in the ion pairing. At a larger distance, $r > 2\sigma$, the charge−charge correlation function $g_{PA+,PE-}$ approaches the average polymer concentration. The two peaks exist for all charge sequences along polyampholyte backbone. However, their magnitudes show a strong charge sequence dependence. The first two peaks have largest magnitudes in the case of long blocky charge sequences, and their magnitude gradually decreases with decreasing the length of uniformly charged blocks along polyampholyte backbone.

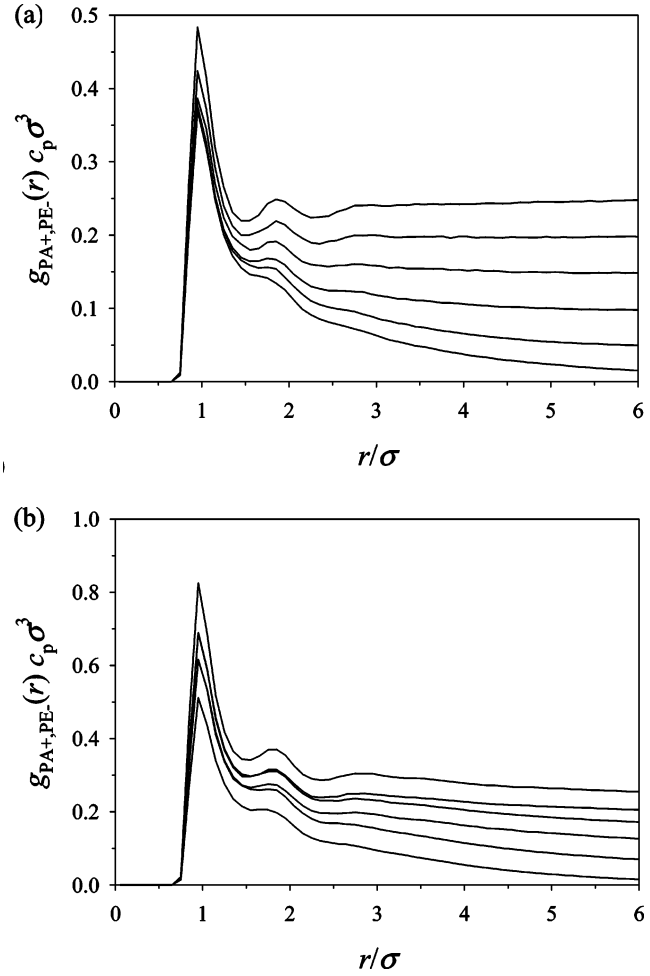

Figure 16. Charge−charge pair correlation function partial pair $g_{PA+,PE-}(r)$ between positively charged beads of polyampholyte and negatively charge beads of polyelectrolyte for (a) RPA−PE and (b) 2B16PA−PE aggregates at different polymer concentrations $c_p = 5 \times 10^{-3}\sigma^{-3}$, $5 \times 10^{-3}\sigma^{-3}$, $10^{-1}\sigma^{-3}$, $1.5 \times 10^{-1}\sigma^{-3}$, $2 \times 10^{-1}\sigma^{-3}$, and $2.5 \times 10^{-1}\sigma^{-3}$ from bottom to top.

In solutions of charged polymers the main contribution to the osmotic pressure of the system comes from small ions.[32−41] Thus, the charge sequence along a polymer backbone should have no effect on the solution osmotic pressure. To verify this fact, we plot the dependence of the osmotic coefficient—ratio of the system osmotic pressure Π to the osmotic pressure of the ideal gas of the counterions $c_p k_B T$ (see Figure 17). All the points collapse into one universal line, confirming the fact that osmotic pressure is dominated by counterions. At low polymer concentrations $c_p < 1.5 \times 10^{-2}\sigma^{-3}$, the osmotic coefficient decreases with increasing polymer concentration. The decrease in the osmotic coefficient indicates the increase in fraction of the condensed counterions. It is worth pointing out that only free counterions contribute to the solution osmotic pressure. The osmotic coefficient starts to increase with polymer concentration in semidilute and concentrated polymer solutions. There are two factors that lead to an increase of the osmotic coefficient with polymer concentration. The first factor is the polymeric contribution to the osmotic pressure, and the second one is the free volume available to counterions and polymer chains. With increasing polymer concentration the available free volume decreases, thus resulting in the hard-sphere

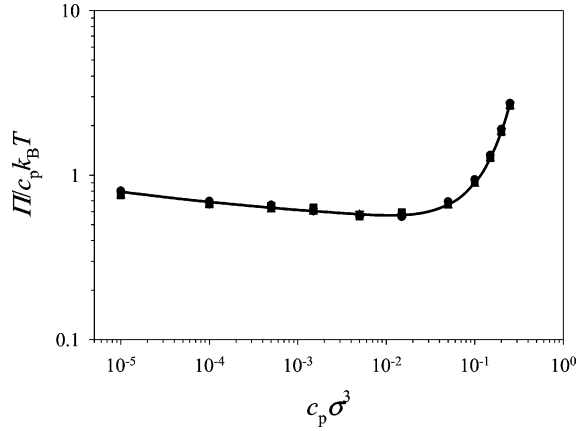

Figure 17. Concentration dependence of the osmotic coefficient for RPA−PE (filled circles), 8B4PA−PE (filled reverse triangles), 4B8PA−PE (filled squares), and 2B16PA−PE (filled triangles).

part of the osmotic pressure providing the significant portion of the system's osmotic pressure.

4. Conclusions

We have studied the effect of the charge sequence along a polyampholyte backbone on complexation in solutions of polyelectrolyte and polyampholyte chains. Using molecular dynamics simulations, we have confirmed the fact that the aggregation between polyampholyte and polyelectrolyte chains proceeds by the polarization-induced attraction mechanism. The ionic groups of both polymers are redistributed in such a way as to maximize the electrostatic attraction between oppositely charged groups and at the same time to minimize the electrostatic repulsion between similarly charged ones. For example, in dilute solutions a diblock polyampholyte and polyelectrolyte can form a three-arm starlike complex in which the longest braches of the star could be formed either by two tails of the polyelectrolyte chain or by a negatively charged block of polyampholyte and by section of polyelectrolyte chain. The middle bead of the star consists of the collapsed sections of polyelectrolyte chain and oppositely charged half of the diblock polyampholyte. These complex structures optimize the electrostatic interactions between ionic groups of both chains and are due to the perfect match between a charge distribution in one-half of the polyelectrolyte chain and in a similarly charged polyampholyte block. These two chains' sections are mutually interchangeable. However, for random polyampholytes or for a block polyampholyte with short blocky sequences there is only one type of the complex. Thus, the hidden symmetry of two chains forming a complex could be broken either by changing the effective linear charged density in two halves of the chains, which is the case for random polyampholytes, or by shortening the block lengths of regular block polyampholytes. In complexes formed by such chains a more positively charged section of polyampholyte chain complexes with part of the polyelectrolyte while the similarly charged part of polyampholyte is pointing away from the polyelectrolyte backbone (see Figure 8). Increasing counterion concentration first leads to the screening of the electrostatic repulsion between elongated sections of polyelectrolyte and polyampholyte chains. This changes the balance of electrostatic interactions in a complex and results a displacement of the collapsed part of the complex toward the center of

the polyelectrolyte backbone. In the case of diblock polyampholytes, the screening of electrostatic repulsion by the salt ions leads to formation of the symmetric three-arm complex.

In dilute solutions of moderate polymer concentrations, multichain aggregates begin to appear (see Figure 9). The probability of finding multichain aggregates gradually increases with polymer concentration. Eventually, at relatively high polymer concentrations, these aggregates span the entire system. Diblock and tetrablock polyampholytes form micellar aggregates that consist of nine chains. The core of these micelles is neutral while all excess polymeric charge is located in the corona of the micelle (see Figures 13 and 14). For random polyampholyte and block polyampholytes 8B4PA the aggregate asymmetry hardly exceeds 2:1 ratio. This asymmetry could be larger for diblock polyampholytes which can form aggregates with 3:1 and 1:3 chain's ratio. The reason for formation of such asymmetric aggregates is once again the inherited symmetry of the diblock polyampholyte and polyelectrolyte chains. The formation of the ionic pairs between oppositely charged ionic groups on both chains could be circled out as one of the factors responsible for strong complexation between polyampholyte and polyelectrolyte chains (see Figure 16). The ionic pairs have higher probability of formation for polyampholyte chains with long blocky charge sequences than for random polyampholytes or polyampholytes with short blocky charge sequences. This indicates the possibility of cooperative effect in ion pair formation.

The osmotic coefficient in polyampholyte−polyelectrolyte mixtures exhibits a nonmonotonic dependence on polymer concentration (see Figure 17). It decreases with increasing polymer concentration in dilute solutions and begins to increase at high polymer concentrations. The upturn in the osmotic coefficient occurs around the overlap concentration. This nonmonotonic dependence of the osmotic coefficient is a general feature of the solutions of ion containing polymers and is a result of the dominant contribution of counterions to solution osmotic pressure. We have also established that the osmotic coefficient does not depend on the distribution of ionic groups along the polymer backbone (see Figure 17).

Acknowledgment. This work was supported by the National Science Foundation under Grant DMR-0305203.

References and Notes

(1) Xia, J.; Dubin, P. L. In *Macromoleculear Complexes in Chemistry and Biology*; Dubin, P., Bock, J., Davis, R., Schluz, D. N., Thies, C., Eds.; Springer-Verlag: Berlin, 1994.
(2) Dubin, P.; Gao, J.; Mattison, K. *Sep. Purif. Methods* **1994**, *23*, 1.
(3) Jiang, J.; Prausnitz, J. M. *J. Phys. Chem. B* **1999**, *103*, 5560.
(4) Jiang, J.; Prausnitz, J. M. *J. Phys. Chem. B* **2000**, *104*, 7197.
(5) Muller, M.; Brissova, M.; Rieser, T.; Powers, A. C.; Lunkwitz, K. *Mater. Sci. Eng.* **1999**, *C8−9*, 163.
(6) Griffith, A.; Glidle, A.; Cooper, J. M. *Biosens. Bioelectron.* **1996**, *11*, 625.
(7) Kokufuta, E. *Prog. Polym. Sci.* **1992**, *174*, 647.
(8) Howe, A. M. *Curr. Opin. Colloid Interface* **2000**, *5*, 288.
(9) Mathews, C. K.; Van Holde, K. E. *Biochemistry*; Benjamin/Cummings: Redwood City, 1990.
(10) Marky, N. L.; Manning, G. S. *J. Am. Chem. Soc.* **2001**, *122*, 6057.
(11) Jayaram, B.; McConnell, K.; Dixit, S. B.; Das, A.; Beveridge, D. L. *J. Comput. Chem.* **2002**, *23*, 1.
(12) Bowman, W. A.; Rubinstein, M.; Tan, J. S. *Macromolecules* **1997**, *30*, 3262.
(13) Swann, D. A.; Caulfield, J. B.; Ceselski, A. *Ann. Rheum. Dis.* **1975**, *34 Supp.*, 98.
(14) Swann, D. A.; Caulfield, J. B. *Conn. Tiss. Res.* **1975**, *4*, 31.
(15) Swann, D. A. In *The Joints and Synovial Fluid*; Sokoloff, L., Ed.; Academic Press: New York, 1978; p 407.
(16) Krause, W. E. Solution Dynamics of Synthetic and Natural Polyelectrolytes. Ph.D. Thesis, Pennsylvania State University, 2000.
(17) Rubinstein, M.; Dobrynin, A. V. *Curr. Opin. Colloid Interface* **1999**, *4*, 83.
(18) Colby, R. H. Polyelectrolyte Interactions with Surfactants and Proteins; Proceedings of the XIIIth International Congress on Rheology, 2000.
(19) Seyrec, E.; Dubin, P. L.; Tribet, C.; Gamble, E. A. *Biomacromolecules* **2003**, *4*, 273.
(20) Hattori, T.; Hallberg, R.; Dubin, P. L. *Langmuir* **2000**, *16*, 9738.
(21) Record, M. T.; Lohman, T. M.; de Haseth, P. *J. Mol. Biol.* **1976**, *107*, 145.
(22) Record, M. T.; Anderson, C. F.; Lohman, T. M. *Q. Rev. Biophys. II* **1978**, *2*, 103.
(23) Mascotti, D. P.; Lohman, T. M. *Proc. Natl. Acad. Sci. U.S.A.* **1990**, *87*, 3142.
(24) Jayaram, B.; DiCapua, F. M.; Beveridge, D. L. *J. Am. Chem. Soc.* **1991**, *113*, 5211.
(25) Giudice, E.; Lavery, R. *Acc. Chem. Res.* **2002**, *35*, 350.
(26) Cheatham, T. E. I.; Young, M. A. *Biopolymers* (*Nucleic Acid Sciences*) **2001**, *56*, 232.
(27) Carlsson, F.; Linse, P.; Malmsten, M. *J. Phys. Chem. B* **2001**, *105*, 9040.
(28) Carlsson, F.; Malmsten, M.; Linse, P. *J. Am. Chem. Soc.* **2003**, *125*, 3140.
(29) Jeon, J.; Dobrynin, A. V. *Phys. Rev. E* **2003**, *67*, 0618031.
(30) Grest, G.; Murat, M. *Macromolecules* **1993**, *26*, 3018.
(31) Plimpton, S. *J. Comput. Phys.* **1995**, *117*, 1.
(32) Kakehashi, R.; Yamazoe, H.; Maeda, H. *Colloid Polym. Sci.* **1998** *276*, 28.
(33) Kakehashi, R.; Maeda, H. *J. Chem. Soc., Faraday Trans.* **1996**, *92*, 3117.
(34) Raspaud, E.,; de Conceicao, M.; Livolant, F. *Phys. Rev. Lett.* **2000**, *84*, 2533.
(35) Hansen, P. L.; Podgornik, R.; Parsegian, A. V. *Phys. Rev. E* **1997**, *64*, 021907-1.
(36) Wang, L.; Bloomfield, V. A. *Macromolecules* **1990**, *23*, 804.
(37) Barrat, J. L.; Joanny, J. F. *Adv. Chem. Phys.* **1996**, *94*, 1.
(38) Dobrynin, A. V.; Colby, R. H.; Rubinstein, M. *Macromolecules* **1995**, *28*, 1859.
(39) Stevens, M. J.; Kremer, K. *J. Chem. Phys.* **1995**, *103*, 1669.
(40) Dobrynin, A. V. In *Simulation Methods for Polymers*; Kotelyanskii, M., Theodorou, D. N., Eds.; Marcel Dekker: New York, 2004; pp 259−312.
(41) Liao, Q.; Dobrynin, A. V.; Rubinstein, M. *Macromolecules* **2003**, *36*, 3399.

MA050303J